

1 Improvement in Fast Particle Track Reconstruction
2 with Robust Statistics

3 M. G. Aartsen², R. Abbasi²⁷, Y. Abdou²², M. Ackermann⁴¹, J. Adams¹⁵,
4 J. A. Aguilar²¹, M. Ahlers²⁷, D. Altmann⁹, J. Auffenberg²⁷, X. Bai^{31,1},
5 M. Baker²⁷, S. W. Barwick²³, V. Baum²⁸, R. Bay⁷, J. J. Beatty^{17,18},
6 S. Bechet¹², J. Becker Tjus¹⁰, K.-H. Becker⁴⁰, M. Bell³⁸,
7 M. L. Benabderrahmane⁴¹, S. BenZvi²⁷, J. Berdermann⁴¹, P. Berghaus⁴¹,
8 D. Berley¹⁶, E. Bernardini⁴¹, A. Bernhard³⁰, D. Bertrand¹², D. Z. Besson²⁵,
9 G. Binder^{8,7}, D. Bindig⁴⁰, M. Bissok¹, E. Blaufuss¹⁶, J. Blumenthal¹,
10 D. J. Boersma³⁹, S. Bohaichuk²⁰, C. Boehm³⁴, D. Bose¹³, S. Böser¹¹,
11 O. Botner³⁹, L. Brayeur¹³, H.-P. Bretz⁴¹, A. M. Brown¹⁵, R. Bruijn²⁴,
12 J. Brunner⁴¹, M. Carson²², J. Casey⁵, M. Casier¹³, D. Chirkin²⁷,
13 A. Christov²¹, B. Christy¹⁶, K. Clark³⁸, F. Clevermann¹⁹, S. Coenders¹,
14 S. Cohen²⁴, D. F. Cowen^{38,37}, A. H. Cruz Silva⁴¹, M. Danninger³⁴,
15 J. Daughhetee⁵, J. C. Davis¹⁷, C. De Clercq¹³, S. De Ridder²², P. Desiati²⁷,
16 M. de With⁹, T. DeYoung³⁸, J. C. Díaz-Vélez²⁷, M. Dunkman³⁸, R. Eagan³⁸,
17 B. Eberhardt²⁸, J. Eisch²⁷, R. W. Ellsworth¹⁶, S. Euler¹, P. A. Evenson³¹,
18 O. Fadiran²⁷, A. R. Fazely⁶, A. Fedynitch¹⁰, J. Feintzeig²⁷, T. Feusels²²,
19 K. Filimonov⁷, C. Finley³⁴, T. Fischer-Wasels⁴⁰, S. Flis³⁴, A. Franckowiak¹¹,
20 R. Franke⁴¹, K. Frantzen¹⁹, T. Fuchs¹⁹, T. K. Gaisser³¹, J. Gallagher²⁶,
21 L. Gerhardt^{8,7}, L. Gladstone²⁷, T. Glüsenkamp⁴¹, A. Goldschmidt⁸,
22 G. Golup¹³, J. A. Goodman¹⁶, D. Góra⁴¹, D. Grant²⁰, A. Groß³⁰,
23 M. Gurtner⁴⁰, C. Ha^{8,7}, A. Haj Ismail²², P. Hallen¹, A. Hallgren³⁹,
24 F. Halzen²⁷, K. Hanson¹², D. Heereman⁴², P. Heimann¹, D. Heinen¹,
25 K. Helbing⁴⁰, R. Hellauer¹⁶, S. Hickford¹⁵, G. C. Hill², K. D. Hoffman¹⁶,
26 R. Hoffmann⁴⁰, A. Homeier¹¹, K. Hoshina²⁷, W. Huelsnitz^{16,2}, P. O. Hulth³⁴,
27 K. Hultqvist³⁴, S. Hussain³¹, A. Ishihara¹⁴, E. Jacobi⁴¹, J. Jacobsen²⁷,
28 K. Jagielski¹, G. S. Japaridze⁴, K. Jero²⁷, O. Jlelati²², B. Kaminsky⁴¹,
29 A. Kappes⁹, T. Karg⁴¹, A. Karle²⁷, J. L. Kelley²⁷, J. Kiryluk³⁵, F. Kislak⁴¹,
30 J. Kläs⁴⁰, S. R. Klein^{8,7}, J.-H. Köhne¹⁹, G. Kohnen²⁹, H. Kolanoski⁹,
31 L. Köpke²⁸, C. Kopper²⁷, S. Kopper⁴⁰, D. J. Koskinen³⁸, M. Kowalski¹¹,
32 M. Krasberg²⁷, K. Krings¹, G. Kroll²⁸, J. Kunnen¹³, N. Kurahashi²⁷,
33 T. Kuwabara³¹, M. Labare¹³, H. Landsman²⁷, M. J. Larson³⁶,
34 M. Lesiak-Bzdak³⁵, M. Leuermann¹, J. Leute³⁰, J. Lünemann²⁸, J. Madsen³³,
35 R. Maruyama²⁷, K. Mase¹⁴, H. S. Matis⁸, F. McNally²⁷, K. Meagher¹⁶,

*Corresponding author. Email: wellons@icecube.wisc.edu, Phone: 304-542-4464, Address: Wisconsin Institutes for Discovery, 330 N. Orchard St., Madison, WI 53715

¹Physics Department, South Dakota School of Mines and Technology, Rapid City, SD 57701, USA

²Los Alamos National Laboratory, Los Alamos, NM 87545, USA

³also Sezione INFN, Dipartimento di Fisica, I-70126, Bari, Italy

⁴Department of Physics, Sungkyunkwan University, Suwon 440-746, Korea

⁵NASA Goddard Space Flight Center, Greenbelt, MD 20771, USA

36 M. Merck²⁷, P. Mészáros^{37,38}, T. Meures¹², S. Miarecki^{8,7}, E. Middell⁴¹,
 37 N. Milke¹⁹, J. Miller¹³, L. Mohrmann⁴¹, T. Montaruli^{21,3}, R. Morse²⁷,
 38 R. Nahnhauser⁴¹, U. Naumann⁴⁰, H. Niederhausen³⁵, S. C. Nowicki²⁰,
 39 D. R. Nygren⁸, A. Obertacke⁴⁰, S. Odrowski³⁰, A. Olivas¹⁶, M. Olivo¹⁰,
 40 A. O’Murchadha¹², L. Paul¹, J. A. Pepper³⁶, C. Pérez de los Heros³⁹,
 41 C. Pfindner¹⁷, D. Pieloth¹⁹, N. Pirk⁴¹, J. Posselt⁴⁰, P. B. Price⁷,
 42 G. T. Przybylski⁸, L. Rädcl¹, K. Rawlins³, P. Redl¹⁶, R. Reimann¹,
 43 E. Resconi³⁰, W. Rhode¹⁹, M. Ribordy²⁴, M. Richman¹⁶, B. Riedel²⁷,
 44 J. P. Rodrigues²⁷, C. Rott¹⁷, T. Ruhe¹⁹, B. Ruzybayev³¹, D. Ryckbosch²²,
 45 S. M. Saba¹⁰, T. Salameh³⁸, H.-G. Sander²⁸, M. Santander²⁷, S. Sarkar³²,
 46 K. Schatto²⁸, M. Scheel¹, F. Scheriau¹⁹, T. Schmidt¹⁶, M. Schmitz¹⁹,
 47 S. Schoenen¹, S. Schöneberg¹⁰, L. Schönherr¹, A. Schönwald⁴¹, A. Schukraft¹,
 48 L. Schulte¹¹, O. Schulz³⁰, D. Seckel³¹, S. H. Seo³⁴, Y. Sestayo³⁰,
 49 S. Seunarine³³, C. Sheremata²⁰, M. W. E. Smith³⁸, M. Soiron¹, D. Soldin⁴⁰,
 50 G. M. Spiczak³³, C. Spiering⁴¹, M. Stamatikos^{17,5}, T. Stanev³¹, A. Stasik⁴¹,
 51 T. Stezelberger⁸, R. G. Stokstad⁸, A. Stöbl⁴¹, E. A. Strahler¹³, R. Ström³⁹,
 52 G. W. Sullivan¹⁶, H. Taavola³⁹, I. Taboada⁵, A. Tamburro³¹,
 53 S. Ter-Antonyan⁶, S. Tilav³¹, P. A. Toale³⁶, S. Toscano²⁷, M. Usner¹¹,
 54 D. van der Drift^{8,7}, N. van Eijndhoven¹³, A. Van Overloop²², J. van Santen²⁷,
 55 M. Vehringer¹, M. Voge¹¹, M. Vraeghe²², C. Walck³⁴, T. Waldenmaier⁹,
 56 M. Wallraff¹, R. Wasserman³⁸, Ch. Weaver²⁷, M. Wellons^{27,*}, C. Wendt²⁷,
 57 S. Westerhoff²⁷, N. Whitehorn²⁷, K. Wiebe²⁸, C. H. Wiebusch¹,
 58 D. R. Williams³⁶, H. Wissing¹⁶, M. Wolf³⁴, T. R. Wood²⁰, K. Woschnagg⁷,
 59 C. Xu³¹, D. L. Xu³⁶, X. W. Xu⁶, J. P. Yanez⁴¹, G. Yodh²³, S. Yoshida¹⁴,
 60 P. Zarzhitsky³⁶, J. Ziemann¹⁹, S. Zierke¹, A. Zilles¹, M. Zoll³⁴, B. Recht⁴²,
 61 C. Ré⁴²

62 ¹III. Physikalisches Institut, RWTH Aachen University, D-52056 Aachen, Germany

63 ²School of Chemistry & Physics, University of Adelaide, Adelaide SA, 5005 Australia

64 ³Dept. of Physics and Astronomy, University of Alaska Anchorage, 3211 Providence Dr.,
 65 Anchorage, AK 99508, USA

66 ⁴CTSPS, Clark-Atlanta University, Atlanta, GA 30314, USA

67 ⁵School of Physics and Center for Relativistic Astrophysics, Georgia Institute of
 68 Technology, Atlanta, GA 30332, USA

69 ⁶Dept. of Physics, Southern University, Baton Rouge, LA 70813, USA

70 ⁷Dept. of Physics, University of California, Berkeley, CA 94720, USA

71 ⁸Lawrence Berkeley National Laboratory, Berkeley, CA 94720, USA

72 ⁹Institut für Physik, Humboldt-Universität zu Berlin, D-12489 Berlin, Germany

73 ¹⁰Fakultät für Physik & Astronomie, Ruhr-Universität Bochum, D-44780 Bochum,
 74 Germany

75 ¹¹Physikalisches Institut, Universität Bonn, Nussallee 12, D-53115 Bonn, Germany

76 ¹²Université Libre de Bruxelles, Science Faculty CP230, B-1050 Brussels, Belgium

77 ¹³Vrije Universiteit Brussel, Dienst ELEM, B-1050 Brussels, Belgium

78 ¹⁴Dept. of Physics, Chiba University, Chiba 263-8522, Japan

79 ¹⁵Dept. of Physics and Astronomy, University of Canterbury, Private Bag 4800,
 80 Christchurch, New Zealand

81 ¹⁶Dept. of Physics, University of Maryland, College Park, MD 20742, USA

82 ¹⁷Dept. of Physics and Center for Cosmology and Astro-Particle Physics, Ohio State
 83 University, Columbus, OH 43210, USA

84 ¹⁸Dept. of Astronomy, Ohio State University, Columbus, OH 43210, USA

85 ¹⁹Dept. of Physics, TU Dortmund University, D-44221 Dortmund, Germany

- 86 ²⁰Dept. of Physics, University of Alberta, Edmonton, Alberta, Canada T6G 2E1
87 ²¹Département de physique nucléaire et corpusculaire, Université de Genève, CH-1211
88 Genève, Switzerland
89 ²²Dept. of Physics and Astronomy, University of Gent, B-9000 Gent, Belgium
90 ²³Dept. of Physics and Astronomy, University of California, Irvine, CA 92697, USA
91 ²⁴Laboratory for High Energy Physics, École Polytechnique Fédérale, CH-1015 Lausanne,
92 Switzerland
93 ²⁵Dept. of Physics and Astronomy, University of Kansas, Lawrence, KS 66045, USA
94 ²⁶Dept. of Astronomy, University of Wisconsin, Madison, WI 53706, USA
95 ²⁷Dept. of Physics and Wisconsin IceCube Particle Astrophysics Center, University of
96 Wisconsin, Madison, WI 53706, USA
97 ²⁸Institute of Physics, University of Mainz, Staudinger Weg 7, D-55099 Mainz, Germany
98 ²⁹Université de Mons, 7000 Mons, Belgium
99 ³⁰T.U. Munich, D-85748 Garching, Germany
100 ³¹Bartol Research Institute and Department of Physics and Astronomy, University of
101 Delaware, Newark, DE 19716, USA
102 ³²Dept. of Physics, University of Oxford, 1 Keble Road, Oxford OX1 3NP, UK
103 ³³Dept. of Physics, University of Wisconsin, River Falls, WI 54022, USA
104 ³⁴Oskar Klein Centre and Dept. of Physics, Stockholm University, SE-10691 Stockholm,
105 Sweden
106 ³⁵Department of Physics and Astronomy, Stony Brook University, Stony Brook, NY
107 11794-3800, USA
108 ³⁶Dept. of Physics and Astronomy, University of Alabama, Tuscaloosa, AL 35487, USA
109 ³⁷Dept. of Astronomy and Astrophysics, Pennsylvania State University, University Park,
110 PA 16802, USA
111 ³⁸Dept. of Physics, Pennsylvania State University, University Park, PA 16802, USA
112 ³⁹Dept. of Physics and Astronomy, Uppsala University, Box 516, S-75120 Uppsala, Sweden
113 ⁴⁰Dept. of Physics, University of Wuppertal, D-42119 Wuppertal, Germany
114 ⁴¹DESY, D-15735 Zeuthen, Germany
115 ⁴²Dept. of Computer Sciences, University of Wisconsin, Madison, WI 53706, USA

116 **Abstract**

117 The IceCube detector is a high-energy neutrino telescope located at the geo-
118 graphic South Pole. Neutrinos cannot be directly observed and must be inferred
119 from their interactions with other particles. These interactions sometimes gen-
120 erate a muon, which in turn emits observable light. At the energies the IceCube
121 detector is sensitive to, the neutrino and generated muon have almost parallel
122 tracks, so the neutrino track can be extrapolated from a reconstruction of the
123 muon track. However, reconstructing the muon track from the observed light is
124 challenging due to noise, light scattering in the ice medium, and the possibility
125 of simultaneously having multiple muons inside the detector.

126 This manuscript describes work on two problems: (1) the *track reconstruction*
127 *problem*, in which, given a set of observations, the goal is to recover the
128 track of a muon, and (2) the *coincident event problem*, which is to determine
129 how many muons are active in the detector during a time window. Rather
130 than solving these problems by developing more complex physical models, our
131 approach is to augment the detector's current models with data filters and ro-
132 bust statistical techniques. Using the metric of median angular resolution, a

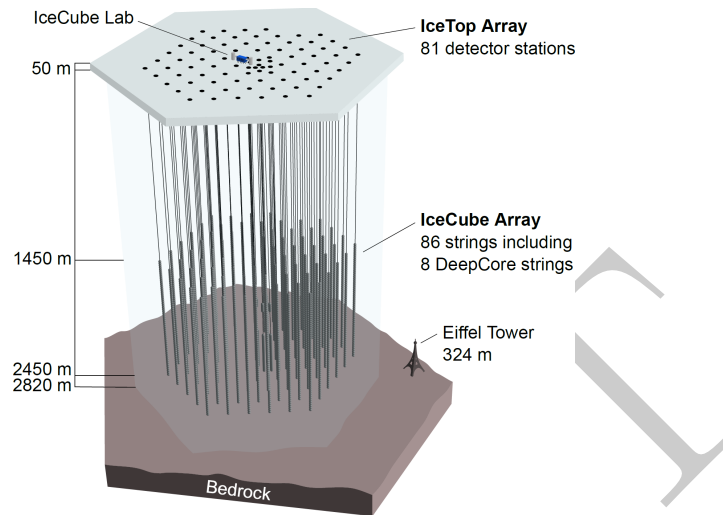


Figure 1: The IceCube neutrino detector in the Antarctic ice. A picture of the Eiffel Tower is shown for scale.

133 standard metric for track reconstruction, we improve the accuracy in the initial
 134 reconstruction direction by 13%. We also present improvements in measuring
 135 the number of muons in coincident events: we can accurately determine the
 136 number of muons 98% of the time, which is an improvement of 86% over the
 137 software previously used in IceCube.

138 *Keywords:* IceCube, Track reconstruction, Neutrino telescope, Neutrino
 139 astrophysics, Robust Statistics

140 **1. Introduction**

141 The IceCube neutrino detector searches for neutrinos that are generated by
 142 the universe’s most violent astrophysical events: exploding stars, gamma ray
 143 bursts, and cataclysmic phenomena involving black holes and neutron stars [1].
 144 The detector, roughly one cubic kilometer in size, is located near the geographic
 145 South Pole and is buried to a depth of about 2.5 km in the Antarctic ice [2].
 146 The detector is illustrated in Figure 1 and a more complete description is given
 147 in Section 2.

148 When a neutrino enters the telescope, it sometimes interacts with the ice and
 149 generates a muon. The neutrino track can be extrapolated from a reconstruction
 150 of the muon track. Muons are also generated by cosmic rays, and separation
 151 of the cosmic ray muons and neutrino muons is a necessary step for neutrino
 152 analysis. This separation is challenging, as the number of observed cosmic

153 ray muons exceeds the number of observed neutrino muons by five orders of
154 magnitude [3].

155 The primary mechanism for separating the cosmic ray muons from the neu-
156 trino muons is reconstructing the muon track and determining whether the
157 muon was traveling downwards into the Earth or upwards out of the Earth.
158 Since neutrinos can penetrate the Earth but cosmic ray muons cannot, it fol-
159 lows that a muon traveling out of the Earth must have been generated by a
160 neutrino. Thus, by selecting only the muons that are reconstructed as up-
161 going, the cosmic ray muons can, in principle, be removed from the data. Since
162 the number of cosmic ray muons overwhelms the number of neutrino muons,
163 high accuracy is critical for preventing erroneous reconstruction of cosmic ray
164 muons as neutrino-induced.

165 Here, we examine two problems that arise in the separation of cosmic ray
166 muons from neutrino muons in the IceCube detector:

- 167 1. *Reconstruction*, in which the track of a muon is reconstructed from the
168 observed light at different positions and times in the detector.
- 169 2. *Coincident Event Detection*, in which we detect the number of muons
170 inside the detector, and assign observed photons to a muon.

171 Previous work on these problems includes developing sophisticated recon-
172 struction models that take into account the interaction of near- and far-field
173 effects of light and mapping photon propagation in the ice [3–5]. The work in
174 this manuscript is focused on refining the statistical techniques and data filtering
175 in the track reconstruction.

176 1.1. Related Work

177 Track reconstruction and coincident event detection challenges are ubiqui-
178 tous in particle physics [6–8], both in particle accelerators and cosmic particle
179 detectors. While the work described in this manuscript builds on the previous
180 technique developed for the IceCube detector [3], these techniques are general
181 purpose, and potentially have applications in detectors beyond IceCube.

182 1.2. Outline

183 We begin by describing the IceCube detector and track reconstruction chal-
184 lenges in Section 2. In Section 3, we describe the reconstruction pipeline in-
185 cluding the prior IceCube software, then we present improvements to the online
186 tracking algorithm and discuss the results. Section 4 describes improvements
187 on coincident event detection, and follows a parallel structure to Section 3. We
188 conclude in Section 5.

189 2. IceCube Detector and Track Reconstruction Challenges

190 The IceCube detector is composed of 5,160 optical detectors, each containing
191 of a photomultiplier tube (PMT) and onboard digitizer [9]. The PMTs are
192 spread over 86 vertical strings arranged in a hexagonal shape, with a total

193 instrumented volume of approximately one cubic kilometer. The PMTs on a
194 given string are separated vertically by 17 m, and the string-to-string separation
195 is roughly 125 m.

196 As the muon travels through the detector, it radiates light [10], which is
197 observed by the PMTs and quantized into discrete *hits* [11]. If a sufficient
198 number of hits is recorded within a time window, the hits are collected into an
199 *event*, and the muon track reconstruction algorithm is triggered.

200 There are several challenges for the reconstruction algorithms used in the
201 detector. Varying optical properties of the ice affect reconstruction accuracy,
202 the data may contain outlier hits due to uncorrelated noise, and there are finite
203 computational resources available to tracking code run on-site.

204 *Modeling Difficulties.* The details of the ice’s optical properties are nontrivial to
205 model. Light propagating through the ice is affected by scattering and absorp-
206 tion. These effects cannot be analytically calculated and the optical properties
207 of the ice vary with depth [5].

208 *Noise.* The noise inherent in the data is another challenge. Noise hits can
209 arise either from the thermal background of the photocathode, or from photons
210 generated by radioactive decay inside the PMT [9].

211 *Computational Constraints.* The reconstruction algorithms are also limited in
212 complexity by the computing resources available at the South Pole. The track
213 reconstruction algorithm has to process about 3,000 muons per second, algo-
214 rithms with excessive computational demands are discouraged.

215 3. Reconstruction Improvement

216 As shown in the following, augmenting the reconstruction algorithm with
217 some basic filters and classical data analysis techniques results in significant
218 improvement in the reconstruction algorithm’s accuracy.

219 3.1. Prior IceCube Software

220 The muon track reconstruction process (outlined in Figure 2) starts when the
221 number of detected hits exceeds a preset threshold and initiates data collection.
222 After the initial data are collected, it then passes through a series of basic filters
223 to remove obvious outliers [12].

224 This is followed by a basic reconstruction algorithm, *linefit* [13], which finds
225 the track that minimizes the sum of the squares of the distances between the
226 track and the hits. More formally, assume there are N hits; denote the position
227 and time of the i th hit as \vec{x}_i and t_i , respectively. Let the reconstructed muon
228 track have a velocity of \vec{v} , and let the reconstructed track pass through point
229 \vec{x}_0 at time t_0 . Then linefit reconstruction solves the *least-squares* optimization
230 problem

$$\min_{t_0, \vec{x}_0, \vec{v}} \sum_{i=1}^N \rho_i(t_0, \vec{x}_0, \vec{v})^2, \quad (1)$$

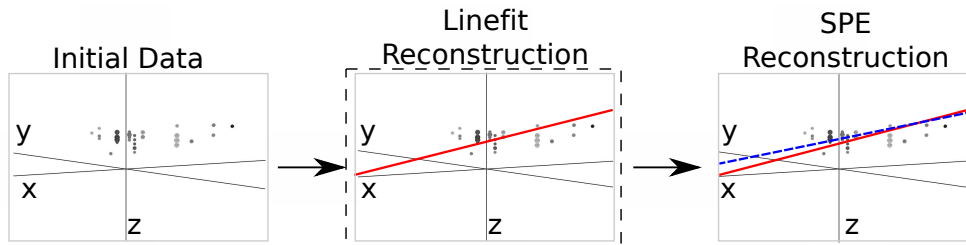


Figure 2: The reconstruction pipeline used to process data in the IceCube detector. After initial data are collected, it is then processed by some basic noise filters, which remove clear outliers. This cleaned data are processed by a basic reconstruction algorithm (solid line), which is used as the seed for the more sophisticated reconstruction algorithm (dashed line). The sophisticated reconstruction is then evaluated as a potential neutrino. The work presented in this manuscript makes changes to the basic reconstruction step (indicated by the dashed box).

231 where

$$\rho_i(t_0, \vec{x}_0, \vec{v}) = \|\vec{v}(t_i - t_0) + \vec{x}_0 - \vec{x}_i\|_2. \quad (2)$$

232 Linefit is primarily used to generate an initial track or *seed* for a more sophis-
 233 ticated reconstruction.

234 The reconstruction algorithm for the sophisticated reconstruction is *Single-*
 235 *Photo-Electron-Fit (SPE fit)* [3]. SPE fit uses the least-squares reconstruction,
 236 the event data, and a parameterized probability distribution function of scatter-
 237 ing in ice [3] to reconstruct the muon track.

238 3.2. Algorithm Improvement

239 SPE fit is dependent on the seed. Given a seed that is inaccurate by 6° or
 240 more, SPE fit typically cannot recover, and produces a reconstruction with the
 241 same level of inaccuracy as the seed track. In addition, the likelihood space for
 242 SPE fit can contain multiple local maxima, so improving the accuracy of a seed
 243 that is already near the true solution improves the accuracy of SPE fit. Thus,
 244 we focus here on improving the quality of the seed.

245 As indicated in Equation 1, a least-squares fit models the muon as a single
 246 point moving in a straight line, and hits are penalized quadratically in their
 247 distance from this line. Thus there is an implicit assumption in this model:
 248 that all the hits will be near the muon. This assumption has two pitfalls:

- 249 1. It ignores the scattering effects of the ice medium. Some of the photons can
 250 scatter for over a microsecond, which means that when they are recorded
 251 by a PMT, the muon will be over 300 m away.
- 252 2. While the noise reduction steps remove most of the outlier noise, the noise
 253 hits that survive can be far from the muon. Since these outliers are given
 254 quadratic weight, they exert a huge influence over the model.

255 The first pitfall occurs because the model is incomplete and does not accu-
 256 rately model the data, and the second demonstrates that the model is not robust

257 to noise. The solution to this is twofold: improve the model and increase the
 258 noise robustness by replacing least squares with robust statistical techniques.

259 3.2.1. Improving the Model

260 The least-squares model does not model the scattering, and thus hits gener-
 261 ated by photons that scattered for a significant length of time are not useful
 262 predictors of the muon’s position. We found that a basic filter could identify
 263 these scattered hits, and improve accuracy by of almost a factor of two by
 264 removing them from the dataset.

265 More formally, for each hit h_i , the algorithm looks at all neighboring hits
 266 within a neighborhood of r , and if there exists a neighboring hit h_j with a time
 267 stamp that is t earlier than h_i , then h_i is considered a scattered hit, and is
 268 not used in the basic reconstruction algorithm. Optimal values of r and t were
 269 found to be 156 m and 778 ns by tuning them on simulated muon data with an
 270 E^{-2} power law spectrum.

271 3.2.2. Adding Robustness to Noise

272 As described in equation 1, the least squares model gives outliers quadratic
 273 weight, whereas we would prefer that outliers had zero weight. There are robust
 274 models in classical statistics designed to marginalize outliers. We experimented
 275 replacing the least-squares model with a Huber fit [14], which improved the
 276 reconstruction accuracy.

277 More formally, we replace Equation 1 with the optimization problem:

$$\min_{t_0, \vec{x}_0, \vec{v}} \sum_{i=1}^N \phi(\rho_i(t_0, \vec{x}_0, \vec{v})), \quad (3)$$

278 where the Huber penalty function $\phi(\rho)$ is defined as

$$\phi(\rho) \equiv \begin{cases} \rho^2 & \text{if } \rho < \mu \\ \mu(2\rho - \mu) & \text{if } \rho \geq \mu \end{cases} . \quad (4)$$

279 Here, $\rho_i(t_0, \vec{x}, \vec{v})$ is defined in Equation 2 and μ is a constant calibrated to the
 280 data (on simulated muon events with an E^{-2} power law spectrum, the optimal
 281 value of μ is 153 m).

282 The Huber penalty function has two regimes. In the near-hit regime ($\rho < \mu$),
 283 hits are assumed to be strongly correlated with the muon’s track, and the Huber
 284 penalty function behaves like least squares, giving these hits quadratic weight.
 285 In the far-hit regime ($\rho \geq \mu$), hits are given linear weights as they are more
 286 likely to be noise.

287 In addition to its attractive robustness properties, the Huber fit’s weight
 288 assignment also has the added benefit that it inherently labels points as outliers
 289 (those with $\rho \geq \mu$). Thus, once the Huber fit is computed, we can go one step
 290 farther and simply remove the labeled outliers from the dataset. A better fit is
 291 then obtained by computing the least-squares fit on the data with the outliers
 292 removed. The entire algorithm has a mean runtime that is approximately six
 293 times slower than Linefit’s mean runtime.

Table 1: Median angular resolution (degrees) for reconstruction improvements. The first line is the accuracy of the prior least-squares model, and the subsequent lines are the accuracy measurements from cumulatively adding improvements into the basic reconstruction algorithm.

Algorithm	θ_{med}
Linefit Reconstruction (Least-Squares)	9.917
With Addition of Logical Filter	5.205
With Addition of Huber Regression	4.672
With Addition of Outlier Removal	4.211

294 3.3. Results

295 The goal is to improve the accuracy of the reconstruction in order to better
 296 separate neutrinos from cosmic rays. Thus we present three measurements: (1)
 297 the accuracy change between linefit and the new algorithm, (2) the accuracy
 298 change when SPE is seeded with the new algorithm instead of linefit, and (3)
 299 the improvement in separation between neutrinos and cosmic rays.

300 To measure the improvement generated by the changes, we use the metric of
 301 *median angular resolution* θ_{med} , which is a standard metric within the collab-
 302 oration. The angular resolution of a reconstruction is the arc-distance between
 303 the reconstruction and the true track. The dataset is drawn from simulated
 304 neutrino data designed to be similar to that observed by the detector.

305 We can improve the median angular resolution of the basic reconstruction
 306 by 57.6%, as shown in Table 1. Seeding SPE with the improved basic recon-
 307 struction generates an improvement in the angular resolution of 12.9%. These
 308 improvements in the reconstruction algorithm result in 10% fewer atmospheric
 309 muons erroneously reconstructed as up-going, and 1% more muons correctly
 310 reconstructed as up-going.

311 4. Coincident Event Improvements

312 In the second study, we look at the problem of determining when more than
 313 one muon has entered the detector. In the most common case, a single muon
 314 will pass through the detector and generate an event before exiting. These events
 315 are processed by the pipeline described in Figure 2. However, for roughly 9%
 316 of the events collected by the data collection algorithm, more than one muon
 317 will be passing through the detector simultaneously, an occurrence known as a
 318 *coincident event*.

319 One of the primary sources of background noise in IceCube analyses is coinci-
 320 dent background muons that have been erroneously reconstructed as neutrinos.
 321 To see why this occurs, consider the coincident event shown in Figure 3. There
 322 are two clear groups of hits; however, the reconstruction algorithm treats them
 323 as a single group, resulting in an erroneous reconstruction. In the ideal case, the
 324 reconstruction algorithm would identify coincident events and split them, as in
 325 Figure 4.

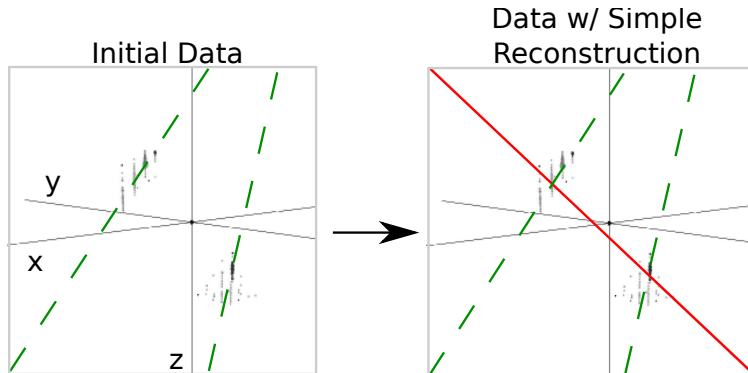


Figure 3: In this example, an event that is clearly composed of two muons (actual tracks shown as dashed lines) is treated as a single muon, and thus the reconstruction (solid line) is inaccurate.

326 The challenge in this example is determining the number of muons in an
 327 event. Our studies show that a simple spatial clustering algorithm can solve
 328 this classification problem with less than 2% error.

329 4.1. Prior IceCube Software

330 Coincident events have been a concern in the IceCube analysis [15] for years,
 331 and some software has been developed to handle coincident events. As a baseline
 332 of comparison, we use the *TTrigger* software, which is described in [16].

333 4.2. Algorithm Improvement

334 Here we present a proximal clustering algorithm. The intuition in proximal
 335 clustering is that points local in space and time are probably from the same
 336 muon. The proximal clustering algorithm iterates through each pair of hits
 337 (i, j) and builds an adjacency matrix \mathbf{A} as

$$\mathbf{A}_{ij} = \begin{cases} 1 & \text{if } \|\Delta x^2 + \Delta y^2 + \Delta z^2 + (c\Delta t)^2\|_2 \leq \alpha, \\ 0 & \text{otherwise} \end{cases} \quad (5)$$

338 where $\Delta x, \Delta y, \Delta z$ and Δt are the space and time differences between the pair
 339 of hits, and α is tuned to the data (in this application, the optimal value of
 340 α is 450 m). The clustering can be recovered by extracting the connected
 341 components of the graph defined by \mathbf{A} . A connected component of a graph is a
 342 subgraph such that there exist a path between any two vertices of this subgraph.

343 4.2.1. Improving the Model

344 When implemented naively, proximal clustering succeeded for the majority
 345 of the events, but failed if there was a gap in the muon track, which can occur
 346 when the muon travels through a dust layer in the ice. If there is a significantly
 347 large gap, the algorithm erroneously separates the hits into two clusters.

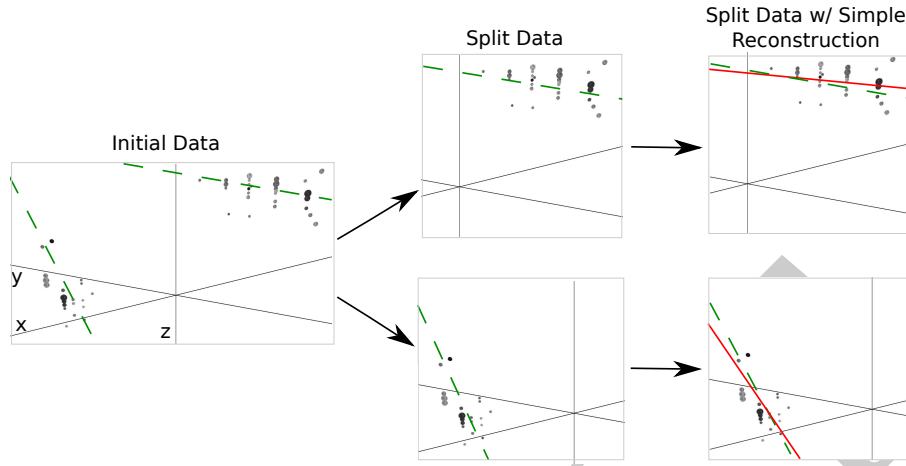


Figure 4: Ideally, the detector would split coincident events before computing the reconstruction. Splitting the event results in more accurate reconstructions (reconstructions shown as solid lines, true muon tracks shown as dashed lines). Note the difference in the reconstructions compared with Figure 3.

348 To get around this, an additional heuristic is added, *track connecting*. Af-
 349 ter the data segmentation is finished, track connecting determines if separate
 350 clusters should be combined. It computes the mean position and time of each
 351 cluster, and connects a hypothetical muon track T between each pair of sub-
 352 spaces.

353 It checks if the speed s of the hypothetical track is within 25% of the speed
 354 of light c , and it checks that the mean distance between hits and T in both
 355 clusters is less than 60 m. If T passes both checks, the clusters are combined.

356 4.2.2. Adding Robustness to Noise

357 Proximal clustering is susceptible to noise. Noise hits close to two disjoint
 358 tracks will be considered adjacent to both tracks, and thus can connect the two
 359 tracks in the adjacency matrix.

360 One heuristic that worked well at mitigating this problem was to not use
 361 all the hits in building the adjacency matrix. During data collection, some hits
 362 are flagged as having a *local coincidence condition*, which indicates that both
 363 they and a neighboring PMT reported a hit. These hits have a high probability
 364 of not being noise hits, and thus exclusively using them to build the adjacency
 365 matrix mitigates the problem of erroneously connecting two tracks.

366 After the proximal clustering algorithm has extracted the tracks from the
 367 adjacency matrix, the hits not used in the construction of the adjacency matrix
 368 are simply assigned to the closest reconstructed track.

369 4.3. Results

370 There were two competing goals for coincident event detection algorithms:
 371 the algorithm should be conservative enough that events containing single tracks

Table 2: Error Rates for Classification Algorithms

Algorithm	$E_{\text{Single}} \%$	$E_{\text{Multiple}} \%$	$E_{\text{tot}} \%$
Trivial	0.0	100.0	8.3
TTrigger	11.5	31.8	13.2
Proximal clustering	0.2	18.9	1.8

372 are not erroneously split, and aggressive enough that a useful fraction of coin-
373 cident events are split correctly. Our algorithm is tuned to keep almost all
374 of the single events correctly unsplit, while still correctly splitting 80% of the
375 coincident events.

376 4.3.1. Measurements

377 We modified the reconstruction pipeline shown in Figure 2, in between the
378 noise cleaning and the basic reconstruction, by adding a step for coincident event
379 detection, as shown in Figure 4. This step takes cleaned data and attempts to
380 classify the event as a single-track or multiple-track event.

381 We ran each algorithm on two datasets of simulated data. One dataset
382 comprised single-muon events, and the other dataset comprised multiple-muon
383 events. In each dataset, we measured the classification error E , which is the
384 fraction of events that were misclassified. To get a global measurement, we
385 compute the *total error* E_{tot} , defined as

$$E_{\text{tot}} = w_{\text{Single}} E_{\text{Single}} + w_{\text{Multiple}} E_{\text{Multiple}}. \quad (6)$$

386 For computing E_{tot} , we use $w_{\text{Single}} = 0.917$ and $w_{\text{Multiple}} = 0.083$, which is
387 the frequency in which single-muon and multiple-muon events appear in data
388 simulating the distribution of events that trigger the reconstruction algorithm.

389 We present the results for the coincident event problem by measuring how
390 well each algorithm performs at determining the number of subspaces in an
391 event.

392 There are two natural comparisons for the work: the prior software TTrigger,
393 as well as the trivial algorithm, which always classifies each event as a single-
394 track event. Clearly, the latter will always get the single-track events correct,
395 and always get the multiple-track events wrong. We provide a comparison of
396 these techniques in Table 2. As shown, the new algorithm classifies the number
397 of muons in the detector 86% better than TTrigger.

398 5. Conclusions

399 We found that significant improvements can be achieved in the IceCube’s on-
400 line track reconstruction by employing some classical data analysis algorithms.
401 Optimizing data filtering and refining the least-square model have led to signif-
402 icant improvements in the accuracy of the reconstruction direction. The new
403 reconstruction software is fast enough to run on-site, and is now included in all
404 IceCube analyses.

405 We also looked at the problem of determining the number of muons in the
406 detector. We found that proximal clustering with some basic heuristics could
407 correctly determine whether an event contained a single muon or multiple muons
408 with less than 2% error, yielding an 86% improvement over the prior software.

409 References

- 410 [1] IceCube Collaboration, IceCube webpage, <http://icecube.wisc.edu/>.
- 411 [2] IceCube Collaboration, First year performance of the IceCube neutrino
412 telescope, *Astroparticle Physics* 26 (3) (2006) 155–173.
- 413 [3] IceCube Collaboration, Muon track reconstruction and data selection tech-
414 niques in AMANDA, *Nuclear Instruments and Methods in Physics Re-*
415 *search Section A* 524 (2004) 169–194.
- 416 [4] IceCube Collaboration, Measurement of South Pole ice transparency with
417 the IceCube LED calibration system IceCube Collaboration, *Nuclear In-*
418 *struments and Methods in Physics Research Section A* (2013) 73–89.
- 419 [5] The AMANDA Collaboration, Optical properties of deep glacial ice at the
420 south pole, *Journal of Geophysical Research* 111 (D13) (2006) D13203.
- 421 [6] ATLAS Collaboration, Tracking and vertexing with the ATLAS detector at
422 the LHC, *Nuclear Instruments and Methods in Physics Research Section A:*
423 *Accelerators, Spectrometers, Detectors and Associated Equipment* 650 (1)
424 (2011) 218–223.
- 425 [7] R. S. Chivukulaa, M. Goldena, E. H. Simmons, Multi-jet physics at hadron
426 colliders, *Nuclear Physics B* 363 (1) (1991) 83–96.
- 427 [8] S. Ellis, J. Huston, K. Hatakeyama, P. Loch, M. Tönnesmann, Jets in
428 hadron–hadron collisions, *Progress in Particle and Nuclear Physics* (60)
429 (2008) 484–551.
- 430 [9] IceCube Collaboration, Calibration and characterization of the IceCube
431 photomultiplier tube, *Nuclear Instruments and Methods in Physics Re-*
432 *search Section A* 618 (2010) 139–152.
- 433 [10] IceCube Collaboration, An improved method for measuring muon energy
434 using the truncated mean of dE/dx , *Nuclear Instruments and Methods in*
435 *Physics Research Section A* 703 (1) (2012) 190–198.
- 436 [11] IceCube Collaboration, The icecube data acquisition system: Signal cap-
437 ture, digitization, and timestamping, *Nuclear Instruments and Methods in*
438 *Physics Research Section A* 601 (3) (2009) 294–316.
- 439 [12] M. Ackermann, Searches for signals from cosmic point-like sources of high
440 energy neutrinos in 5 years of AMANDA-II data, Ph.D. thesis, Humboldt-
441 Universität zu Berlin (2006).

- 442 [13] V. Stenger, Track fitting for DUMAND-II Octagon Array, Tech. rep., Uni-
443 versity of Hawai'i at Manoa (1990).
- 444 [14] S. Boyd, L. Vandenberghe, Convex Optimization, Cambridge University
445 Press, 2009.
- 446 [15] IceCube Collaboration, Measurement of the atmospheric neutrino energy
447 spectrum from 100 GeV to 400 TeV with IceCube, Physical Review D
448 83 (1).
- 449 [16] D. Chirkin, Measurement of the atmospheric neutrino energy spectrum
450 with IceCube, Proceedings of the 31st ICRC.

DRAFT